Available online at www.sciencedirect.com

jmr&t Journal of Materials Research and Technology

journal homepage: www.elsevier.com/locate/jmrt

Original Article

Design of compositionally complex catalysts: Role of surface segregation

Alberto Ferrari [a,b,*], *Fritz Körmann* [b,c]

[a] RUB Research School, Ruhr Universität Bochum, 44801 Bochum, Germany
[b] Materials Science and Engineering, Delft University of Technology, 2628CD Delft, the Netherlands
[c] Max-Planck-Institut für Eisenforschung GmbH, 40237 Düsseldorf, Germany

ARTICLE INFO

Article history:
Received 15 March 2021
Accepted 19 July 2021
Available online 26 July 2021

Keywords:
Compositionally complex alloys
High entropy alloys
Surface segregation

ABSTRACT

Besides revealing excellent mechanical properties, compositionally complex alloys are also very promising candidates for applications in heterogeneous catalysis. The opportunity provided by the tremendously large composition phase space to explore new materials and tune the materials properties in the materials design cycle is, however, intrinsically coupled with the challenge of controlling surface segregation, which is generally more severe in multicomponent alloys as compared to simpler systems. We demonstrate this by computing the surface phase diagram of two candidate compositionally complex catalysts. Significant surface segregation is found even at very high temperature and this can strongly affect the catalytic properties of these alloys. We explain the observed phase stabilities in terms of segregation energies and rationalize the segregation trends with canonical models. Finally, we propose a set of descriptors accessible with first-principles calculations that allows to quickly incorporate the evaluation of the segregation during the alloy design process.

1. Introduction

Materials for electrocatalysis are traditionally based on simple metals or bimetallic alloys. In contrast, compositionally complex alloys (CCAs, often termed high entropy alloys) [1–5] are complex metallic solid solutions with four, five, or more elements in concentrated compositions that, however, retain simple lattices (face-centered cubic, fcc, body-centered cubic, bcc, or close-packed hexagonal, hcp).

The principle that guides the design of materials for electrocatalysis is the optimization of the absorption energy of the reactants and products on the surface of a catalyst (Sabatier principle or vulcano plot principle) [6,7], i.e., the absorption energy must be high enough so that the reactants dissociate effectively at the surface, but low enough to let the products desorb.

Very recently, catalysts based on CCAs [8,9] were shown to outperform state-of-the-art metals for methanol oxidation [10–13], oxygen reduction [13–16], hydrogen evolution [13,17,18], ammonia splitting [19–21], oxygen evolution [16,22], and CO and CO_2 reduction [23] reactions. Possible explanations for this outstanding performance of CCAs are the

* Corresponding author.
E-mail address: A.Ferrari-1@tudelft.nl (A. Ferrari).
https://doi.org/10.1016/j.jmrt.2021.07.084

possibility to better fine-tune the composition to obtain the optimal absorption energy, and the opportunity to perform this fine-tuning for more than one reaction step at once [8].

Despite the remarkable progress for this materials class, a potential issue that may impact the performance of CCA catalysts is surface segregation [24,25]. In contrast to simple metals, the composition of the surface of complex alloys can be rather different from the nominal composition of the bulk because some elements or element combinations may be thermodynamically favored or unfavored at the surface sites. Segregation may enhance or reduce the rate of certain reactions or reaction steps; having control of this phenomenon may turn out to be beneficial to boost some processes, but unwanted segregation shifting the surface composition away from a predetermined optimum could lead to a strong, detrimental decrease in the catalytic activity.

Although many new CCA catalysts were recently proposed [10–23], detailed analysis of surface segregation has often been lacking. The purpose of this work is to quantify the amount of surface segregation in typical noble-metal-based CCAs, to demonstrate that generally it is not negligible, and to present a robust strategy based on first principles calculations to evaluate segregation during the catalyst design process. To exemplify this, we calculate with Density Functional Theory (DFT) the surface phase diagrams of two candidate compositionally complex catalysts, namely $Pt_{55.9}Ir_{22.6}Pd_{9.0}Ru_{8.9}Ag_{3.6}$ (Pt-rich alloy) and $Ir_{47.0}Pt_{29.0}Ru_{12.9}Pd_{9.6}Ag_{1.5}$ (Ir-rich alloy) [26]. Similar compositions were recently studied in Refs. [15,27] in relation to the oxygen reduction reaction. We consider the possibility for oxygen to adsorb on the surface and we estimate the equilibrium coverage of the segregated and unsegregated surfaces as a function of temperature. We show that surface segregation is present at every temperature below melting. Indeed, strong Ru segregation at low temperature (when O can bind to the surface) and Ag segregation at high temperature up to the melting point (under vacuum conditions) are observed. We explain these observations by carefully analyzing the segregation energies of the constituent elements of the two CCAs derived from first principles. We also rationalize the segregation trends in terms of canonical models and suggest practical guidelines to incorporate surface segregation into the design process of multicomponent electrocatalysts.

2. Calculation details

2.1. *Surface phase diagram*

To calculate the surface phase diagram of the two CCAs, we considered a slab with N_s surface atoms arranged in a random configuration (unsegregated slab, with free energy $G^{(ran)}_{slab}$), and a corresponding slab having the surface atoms transmuted into type i (i-segregated slab, with free energy $G^{(i)}_{slab}$). For the surface we chose the (111) orientation. We also contemplated the possibility for O to absorb on the surface, which is likely a stable configuration at low temperature, by modeling $\frac{1}{3}$, $\frac{2}{3}$, and 1 monolayer (ML) of O absorbed at the hollow fcc sites. The interaction among the adsorbed O atoms is taken into account. To quantify the tendency towards segregation for an element i, we evaluated the free energy difference

$$G^{(i)}_{segr} = \frac{1}{N_s}\left[G^{(i)}_{slab} - G^{(ran)}_{slab} - \sum_j \left(n^{(i)}_j - n^{(ran)}_j\right)\mu_j - n_O\mu_O\right], \quad (1)$$

where $n^{(i)}_j = N_s\,\delta_{ij}$ and $n^{(ran)}_j$ are the number of atoms of type j on the i-segregated slab and the unsegregated slab, respectively. The number of O atoms absorbed on the surface (0, $\frac{N_s}{3}$, $\frac{2N_s}{3}$, or N_s) is denoted as n_O, and μ_j is the chemical potential of the element j that balances the energy cost associated with the transmutation of the surface atoms or the addition of O. By rearranging the terms, it can be shown that only chemical potential differences $\Delta\mu_{ij} = \mu_i - \mu_j$ between the constituent elements contribute to the third term in Eq. (1), which we determined in the bulk as [24,28].

$$\Delta\mu_{ij} = \lim_{c\to 0}\frac{1}{c}\left[G_{bulk}(A_{1-c}i_c) - G_{bulk}(A_{1-c}j_c)\right], \quad (2)$$

where G_{bulk} is the free energy of an fcc bulk structure and A denotes the Pt- or Ir-rich alloy. In practice, a finite value of $c = \frac{1}{54} \simeq 1.85\%$ was chosen for the present work. The free energies and chemical potentials in the solid phase were considered based on the first-principles derived total energies and the configurational entropy of a random alloy:

$$G = E - TS + pV \simeq E + k_B T\sum_j c_j \ln c_j. \quad (3)$$

Note that other finite-temperature contributions due to vibrations and electronic excitations are typically negligible as they largely cancel out in Eq. (1).

For estimating μ_O in the gas phase we instead took into account the vibrational, nuclear, rotational, and translational degrees of freedom, as suggested in Ref. [29]. We fixed the oxygen partial pressure in the gas phase to 0.2 atm.

Based on this, the free energy difference in Eq. (1) can be rewritten with Eq. (3) to explicit the temperature dependence as

$$G^{(i)}_{segr}(T) = G^{(i)}_{segr}(0) - k_B T \ln c_i - \mu_O(T), \quad (4)$$

where the temperature dependence of the chemical potential of oxygen $\mu_O(T)$ can be fitted from the data provided in Ref. [29]. We assumed a parabolic dependence of $\mu_O(T)$ and parametrized

$$\mu_O(T) = k_1 T + k_2 T^2 + \frac{1}{2}k_B T \ln 0.2, \quad (5)$$

with $k_1 = -9.44 \cdot 10^{-4}$ eV/K and $k_1 = -1.81 \cdot 10^{-7}$ eV/K^2 and the last term the ideal gas contribution at a partial pressure of 0.2 atm.

For each surface population (segregated with each of the five elements or unsegregated), we estimated the surface coverage at each temperature by fitting the free energies for the four considered coverages with cubic splines and then taking the numerical minimum of the free energy. At higher temperature, μ_O becomes lower and lower and competes with the binding energy, eventually triggering the desorption of oxygen from the surface.

We computed also the segregation energies at the subsurface layer by fixing the configuration of the surface to the thermodynamically most stable one and calculating free energy differences as in Eq. (1).

2.2. Computational setup

The DFT calculations were conducted with the plane-wave projector augmented wave (PAW) method [30,31] as implemented in VASP 5.4 [32–34] with the generalized gradient approximation (PBE) [35]. We employed the same setup as in Ref. [24]. We modeled fcc(111) surfaces with 3 × 3 × 9 slabs with 20 Å of vacuum and used a k-mesh of 6 × 6 × 1. To compute the chemical potentials we used 3 × 3 × 6 supercells with a k-mesh of 6 × 6 × 4. To estimate the statistical uncertainties on the segregation free energies, due to the finite size of the supercells, we took into account 5 different random slabs and 100 different random supercells for each composition and for each element to compute surface energies and chemical potentials, respectively. The equilibrium lattice parameters (3.932 Å and 3.899 Å for the Pt-rich and Ir-rich CCAs, respectively) were found by a Birch-Murnaghan fit [36,37] of energy-volume points. We arranged the adsorbed oxygen atoms for the partial coverages of $\frac{2}{3}$ and $\frac{1}{3}$ ML on a honeycomb pattern and its complementary, respectively, to minimize the lateral interactions between the oxygen atoms.

3. Results

3.1. Segregation at finite temperature

Fig. 1 presents the relative stability of the different surface configurations as a function of temperature for a) the Pt-rich alloy and b) the Ir-rich alloy. The free energy differences (solid lines) are calculated with respect to the random configuration of the surface. The equilibrium coverage for each configuration, resulting from the minimization of the free energy interpolated from the data at 0, $\frac{1}{3}$, $\frac{2}{3}$, and 1 ML, is also reported in Fig. 1. In agreement with previous investigations [38], we find that elements with a low affinity to oxygen, especially Ag, tend to prefer low coverages at low temperature, while a whole ML is instead favored on the Ru-rich surface at low temperature. As expected, the behavior of the random surfaces is intermediate between these two scenarios.

The surface phase diagram of the two CCAs is very similar: in both cases, 1 ML O is absorbed at the surface at low temperature, promoting the segregation of Ru. At temperatures higher than roughly 1100 K and 750 K for the Pt-rich and Ir-rich CCAs, respectively, the segregation of Ag with little or no oxygen is instead preferred. Despite the low concentration of Ag, which tends to lower the chemical potential of this element at finite temperature and hence would hinder the segregation (see Eq. (4)), this element is favored at the surface sites even up to the melting point (here roughly estimated as a weighted average of the melting temperatures of the single elements). Segregation happens because the main driving force towards disorder, the configurational entropy $-k_B\sum_j c_j \ln c_j$, is not strong enough to contrast the large segregation energies of Ru (in the presence of O) and Ag (in vacuum). Consequently, the composition of the surface is predicted to be markedly different from that of the bulk. As already mentioned, due to the limited supercell size, we considered multiple random configurations of the surface and the bulk structures; from these, we obtained statistical errors which result in an uncertainty on the derived transition temperatures of about 150 K but do not qualitatively alter the observed tendencies.

To explain the observed segregation trends, we analyze in detail the segregation energies of the constituent elements of the two CCAs at 0 K in the next subsection.

3.2. Segregation energies

Fig. 2 shows the segregation energies of the constituent elements in the Pt-rich and Ir-rich CCAs in vacuum (Fig. 2a and c) and with 1 ML O absorbed on the surface (Fig. 2b and d). The upper panels refer to the segregation at the outermost layer (surface), the lower panels at the layer immediately below (subsurface).

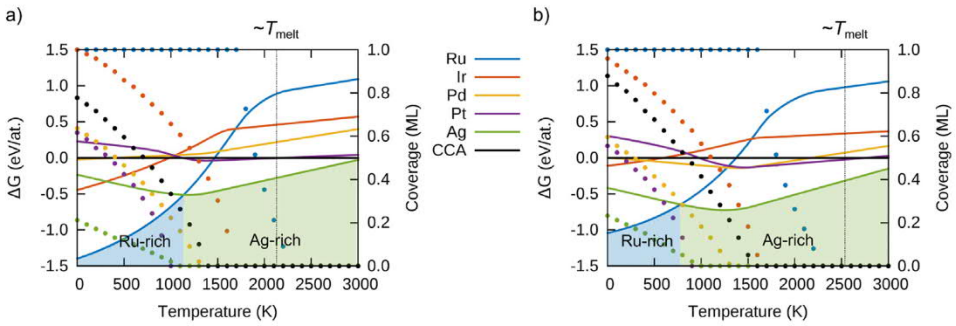

Fig. 1 – Free energy difference with respect to the random state (left scale, solid lines) and surface coverage (right scale, points) of the studied surface configurations as a function of temperature for a) the Pt-rich alloy and b) the Ir-rich alloy. Results are obtained by averaging 100 random bulk supercell configurations and 5 different slab configurations for each composition and for each segregating element. The reported coverages for each temperature are those that minimize the free energy at that temperature. The indicated melting temperature T_{melt} is estimated as a weighted average of the melting temperatures of the constituent elements.

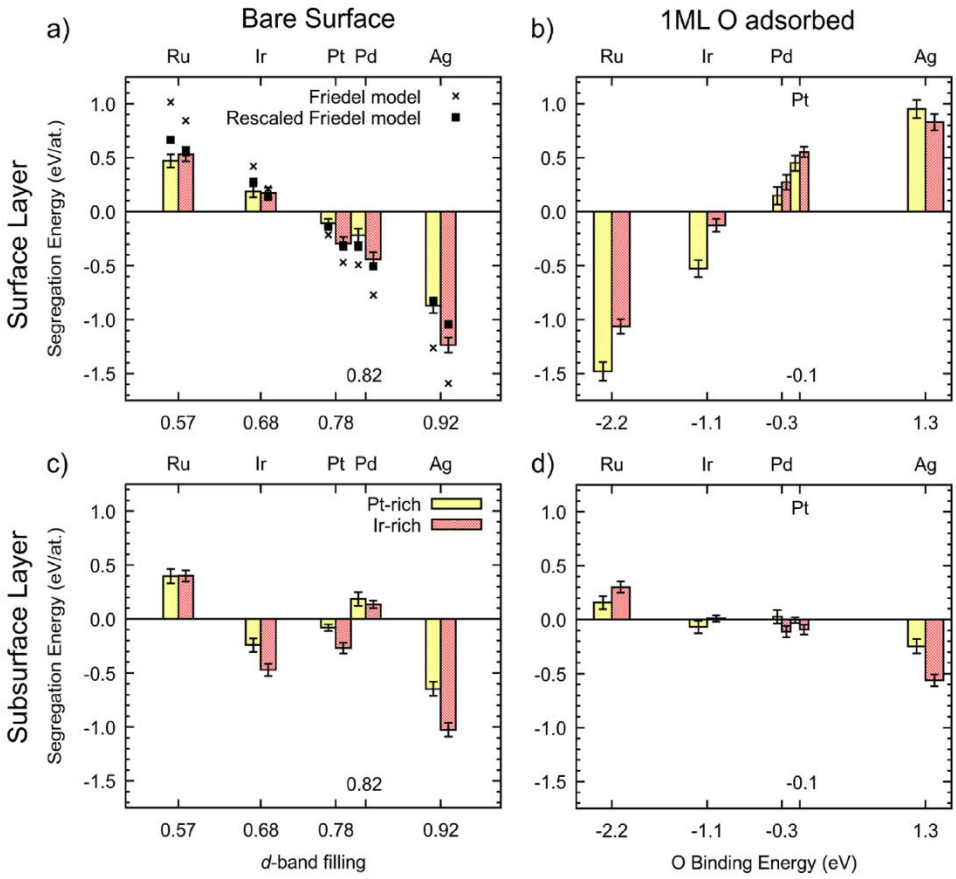

Fig. 2 – Surface segregation for the constituent elements in Ag-Ir-Pd-Pt-Ru: a) for the surface layer in vacuum, b) for the surface layer with 1 ML O, c) for the subsurface layer if the surface layer is occupied by Ag, d) for the subsurface layer if the surface layer is occupied by Ru. The *x*-axes are common descriptors that correlate with the segregation energies: the *d*-band filling of the elements for segregation in vacuum and the oxygen binding energy to the surface of the elements for segregation with O. The statistical error bars account for different atomic configurations. Crosses are the predictions by the Friedel model (see Sec. 3.3), squares are the same values rescaled by 0.655 (see text for details).

In vacuum conditions (Fig. 2a), as already evident from the surface phase diagram, Ag strongly segregates at the surface for both compositions, whereas Ru strongly antisegregates. This result is largely expected, given that Ag and Ru have the lowest (722 mJ/m^2) and highest (2537 mJ/m^2) surface formation energies among the five elements, respectively. Furthermore, Ag has a significantly larger lattice parameter than that of the two CCAs (+5.5% and +6.4% with respect to the Pt-rich and Ir-rich CCAs, respectively), which favors the migration of this element to the surface to release internal strains. The opposite holds for Ru, with a smaller lattice parameter than the two CCAs (−3.1% and −2.3%, respectively).

When Ag segregates to the surface, we observe an enrichment of Ag and Ir at the subsurface layer, with the subsurface segregation of Ag larger than that of Ir (Fig. 2c). At thermodynamic equilibrium, we therefore expect Ag to form a film on the surface, despite the content of this element is only a few at.% for both CCAs.

As anticipated from the surface phase diagram, the situation changes drastically in the presence of O (Fig. 2b). In this case Ru strongly segregates at the surface, whereas Ag strongly antisegregates and Ir, Pd, and Pt take intermediate values for the segregation energy. However, at the subsurface layer (Fig. 2d), Ag is again favored, possibly due to strain-induced contributions, i.e., the small lattice parameter of Ru at the surface needs to be compensated by that of Ag below.

Overall, the results show that surface segregation is very prominent in both CCAs (segregation energies are higher than 1 eV in magnitude) and explain why the resultant surface composition is predicted to be considerably different from the nominal bulk composition even at high temperature. For these systems, strong segregation is typically undesirable, as it may substantially decrease the catalytic performance of the candidate alloys and ultimately invalidate the whole design protocol. To overcome this issue, in the next subsection we propose descriptors that can be used to take into account surface segregation during the alloy design process.

3.3. *Descriptors that correlate with the segregation energy*

Besides surface formation energies and lattice parameters, the trend of the segregation energies in vacuum and in the

presence of reactants can be rationalized using canonical models and/or simple descriptors that can be calculated straightforwardly from first-principles and which can be easily implemented in an alloy design protocol. As detailed in Ref. [24,28], the segregation energy of an element in an alloy in vacuum depends mainly on the *d*-band filling of the element, $f^\star$, and of the alloy f. This dependence can be accounted for using the canonical Friedel model [39], that assumes a rectangular *d*-density of states with bandwith w. For the fcc(111) surface, the Friedel model gives [24,28].

$$E_{segr} = 0.670\, w(f)\,[f^\star\,(1-f^\star) - f\,(1-f)]. \quad (6)$$

We obtained $f^\star$ by integrating the *d*-densities of states of the constituent elements and f and w by a weighted average of the corresponding quantities for the pure elements. w is 6.98 eV and 7.47 eV for the Pt-rich and Ir-rich CCAs, respectively, and the *d*-band fillings for the elements are Ru: 0.57, Ir: 0.68, Pt: 0.78, Pd: 0.82, and Ag: 0.92.

As can be seen in Fig. 2a, the surface segregation energies correlate very clearly with the *d*-band filling (*x*-axis) and the Friedel model (crosses in Fig. 2a) captures qualitatively the segregation trend, despite this simplistic approximation overestimates the magnitude of segregation/antisegregation. Employing an empirical rescaling of the Friedel model predictions (by a factor of 0.655) though provides good agreement (root-mean-squared error of only 0.102 eV) with the DFT segregation energies (squares in Fig. 2a). This rescaling may be interpreted as a homogeneous shrinkage of the *d*-bandwidth, that compensates the crude assumption that the density of states is rectangular in the Friedel model. Although we do not expect this factor to be the same for *any* arbitrary alloy, we already observe that it is reasonably well transferable between the two compositions and likely applicable to the present alloy family.

Using the Friedel model, some peculiar features in the calculated segregation energies can be explained. For instance, the lower segregation energy of Ag in the Ir-rich alloy can partially be ascribed to the fact that this alloy has a smaller lattice parameter, and partially to the fact that it has also a smaller f.

The reason why canonical models such as the Friedel model can make reasonable predictions for CCAs is that the densities of states of these complex alloys are indeed very similar to those of the constituent elements and trends can often be qualitatively explained by considering bandwidth adjustments and rigid shifts of the Fermi level. For instance, Fig. 3 displays the projected densities of *d*-states (PDOS) of Ag, Pd, Pt (upper panel), Ir, Ru, and the Pt-rich CCA (lower panel). The densities of states of the 4*d* elements Ag, Pd and Ru, and the 5*d* elements Pt and Ir can clearly be obtained from each other by dilatation of the bandwidth and shift of the band filling, and the PDOS of the CCA presents intermediate features between the five elements: as the alloy is rich in Pt, the corresponding PDOS is very similar to that of Pt, but distinctive attributes of the PDOSs of the other elements, such as the broadening of the peak at the Fermi level due to Pd and the higher energy peak due to Ir and Ru, can be recognized as well.

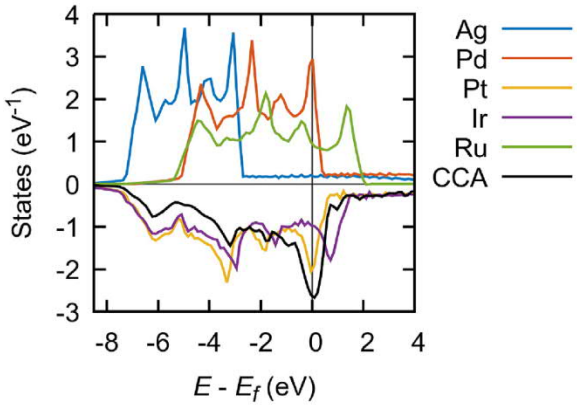

Fig. 3 – Projected density of *d*-states of the 4*d* elements (upper panel) and 5*d* elements and of the Pt-rich alloy (lower panel).

In the presence of O, an intuitive descriptor that correlates with the segregation energy is instead the binding energy of O on the surface of the pure elements, here computed as

$$E_{bind} = \frac{E_{slab-O} - E_{slab} - E_{O_2}}{2}, \quad (7)$$

where $E_{slab\text{-}O}$ and E_{slab} are the energies of slabs with and without O absorbed on the two surfaces, respectively, and E_{O_2} is the total energy of a O_2 molecule.

As observed in Fig. 2b, the segregation energy is approximately linear with respect to E_{bind} (on the *x*-axis). Although it is difficult to predict the magnitude of the segregation energy solely form E_{bind}, during the alloy design process one may limit the choice of the elements to those whose E_{bind} differ by less than a given threshold (a reasonable estimate may be, for instance, 1.5 eV).

It should also be noted that generally reactants bind on the surface of noble metals only at relatively low temperature. In these conditions, diffusion from the bulk to the surface may be kinetically hindered, hence the most stable configuration at high temperature could be retained, even if thermodynamically unstable. This is also the reason why accurately assessing the segregation in vacuum may sometimes be more important.

4. Discussion

Even if the constituent elements of the two alloys studied here were initially chosen close to each other in the periodic table to avoid demixing and precipitation of new phases, our results prove that surface segregation does take place, potentially affecting the functionality of the designed electrocatalysts. The design of new multicomponent materials for electrocatalysis should therefore take segregation effects into account. We propose two alternative strategies: (i) the optimal composition should be chosen to boost the reaction kinetics but also under the constraint of minimizing segregation; (ii) selective segregation could be enhanced and actively exploited to achieve the target composition on the surface, different from the bulk.

To incorporate the evaluation of the segregation energy inside the computational materials design protocol, efficient descriptors from first-principles can be used to boost up the theoretical predictions. The segregation in vacuum can be estimated from bandwidths and band fillings, that both can be very efficiently computed as weighted averages of the bandwidths and band fillings of the individual constituents. The segregation in the presence of reactants such as O can be related to the binding energy of the reactants on the surface of the pure metals. It is found that canonical theories, such as the Friedel model, work well for the considered CCAs because the mixing of the constituent elements in these systems is almost ideal and, as a first approximation, the first few moments of the densities of states can be interpolated from those of the pure elements.

In summary, we calculated the surface phase diagrams of two candidate CCAs for electrocatalysis of the oxygen reduction reaction. At low temperature, when the absorption of O is favorable, Ru tends to segregate at the surface, whereas at high temperature, when O prefers the gas reservoir, Ag segregates. We predict that segregation is thermodynamically favorable even up to the melting point. This is due to the very strong segregation energies of Ru and Ag, that can be rationalized in terms of the *d*-band filling. We propose to take segregation into account during the materials design cycle by exploiting the computationally very efficient Friedel model, that only needs the densities of states of the constituent elements as an input, and the binding energies of the reactants on the pure elements. These findings pave the way for exploiting more active and stable catalysts, crucial for a plethora of applications ranging from energy production and storage over processing of chemicals to sequestration of harmful substances.

Data availability

Derived data supporting the findings of this study are available from the corresponding author upon request.

Declaration of Competing Interest

The authors declare that they have no known competing financial interests or personal relationships that could have appeared to influence the work reported in this paper.

Acknowledgements

This work was supported by the Ruhr University Research School PLUS, funded by Germany's Excellence Initiative [DFG GSC 98/3], and by the Nederlandse Organisatie voor Wetenschappelijk Onderzoek (NWO) [VIDI Grant No. 15707]. A.F. warmly thanks Tom Batchelor (University of Copenhagen) for suggesting the compositions of the CCAs and for helpful discussions. We also kindly acknowledge fruitful discussions with Andrei Ruban (KTH).

REFERENCES

[1] Yeh J-W, Chen S-K, Lin S-J, Gan J-Y, Chin T-S, Shun T-T, et al. Nanostructured high-entropy alloys with multiple principal elements: novel alloy design concepts and outcomes. Adv Eng Mater 2004;6:299–303.
[2] Cantor B, Chang I, Knight P, Vincent A. Microstructural development in equiatomic multicomponent alloys. Mater Sci Eng 2004;375:213–8.
[3] Murty BS, Yeh J-W, Ranganathan S, Bhattacharjee P. High-entropy alloys. Elsevier; 2019.
[4] Ikeda Y, Grabowski B, Körmann F. Ab initio phase stabilities and mechanical properties of multicomponent alloys: a comprehensive review for high entropy alloys and compositionally complex alloys. Mater Char 2019;147:464–511.
[5] Ferrari A, Dutta B, Gubaev K, Ikeda Y, Srinivasan P, Grabowski B, et al. Frontiers in atomistic simulations of high entropy alloys. J of Appl Phys 2020;128:150901.
[6] Nørskov JK, Rossmeisl J, Logadottir A, Lindqvist L, Kitchin JR, Bligaard T, et al. Origin of the overpotential for oxygen reduction at a fuel-cell cathode. J Phys Chem B 2004;108:17886–92.
[7] Bligaard T, Nørskov JK, Dahl S, Matthiesen J, Christensen CH, Sehested J. The Brønsted–Evans–Polanyi relation and the volcano curve in heterogeneous catalysis. J Catal 2004;224:206–17.
[8] Löffler T, Savan A, Garzón-Manjón A, Meischein M, Scheu C, Ludwig A, et al. Toward a paradigm shift in electrocatalysis using complex solid solution nanoparticles. ACS Energy Lett 2019;4:1206–14.
[9] Löffler T, Savan A, Meyer H, Meischein M, Strotkötter V, Ludwig A, et al. Design von komplexen Mischkristall-Elektrokatalysatoren auf Basis der Korrelation von Konfiguration, Verteilungsmustern der Adsorptionsenergie und Aktivitätskurven. Angew Chem 2020;132:5893–900.
[10] Tsai C-F, Wu P-W, Lin P, Chao C-G, Yeh K-Y. Sputter deposition of multi-element nanoparticles as electrocatalysts for methanol oxidation, Japan. J Appl Phys 2008;47:5755.
[11] Wang A-L, Wan H-C, Xu H, Tong Y-X, Li G-R. Quinary PdNiCoCuFe alloy nanotube arrays as efficient electrocatalysts for methanol oxidation. Electrochim Acta 2014;127:448–53.
[12] Chen X, Si C, Gao Y, Frenzel J, Sun J, Eggeler G, et al. Multi-component nanoporous platinum–ruthenium–copper–osmium–iridium alloy with enhanced electrocatalytic activity towards methanol oxidation and oxygen reduction. J Power Sources 2015;273:324–32.
[13] Qiu H-J, Fang G, Wen Y, Liu P, Xie G, Liu X, et al. Nanoporous high-entropy alloys for highly stable and efficient catalysts. J Mater Chem A 2019;7:6499–506.
[14] Löffler T, Meyer H, Savan A, Wilde P, Garzón Manjón A, Chen Y-T, et al. Discovery of a multinary noble metal–free oxygen reduction catalyst. Adv Energy Mater 2018;8:1802269.
[15] Batchelor TA, Pedersen JK, Winther SH, Castelli IE, Jacobsen KW, Rossmeisl J. High-entropy alloys as a discovery platform for electrocatalysis. Joule 2019;3:834–45.
[16] Lacey SD, Dong Q, Huang Z, Luo J, Xie H, Lin Z, et al. Stable multimetallic nanoparticles for oxygen electrocatalysis. Nano Lett 2019;19:5149–58.
[17] Zhang G, Ming K, Kang J, Huang Q, Zhang Z, Zheng X, et al. High entropy alloy as a highly active and stable electrocatalyst for hydrogen evolution reaction. Electrochim Acta 2018;279:19–23.

[18] Glasscott MW, Pendergast AD, Goines S, Bishop AR, Hoang AT, Renault C, et al. Electrosynthesis of high-entropy metallic glass nanoparticles for designer, multi-functional electrocatalysis. Nat Commun 2019;10:1–8.
[19] Yao Y, Huang Z, Xie P, Lacey SD, Jacob RJ, Xie H, et al. Carbothermal shock synthesis of high-entropy-alloy nanoparticles. Science 2018;359:1489–94.
[20] Xie P, Yao Y, Huang Z, Liu Z, Zhang J, Li T, et al. Highly efficient decomposition of ammonia using high-entropy alloy catalysts. Nat Commun 2019;10:1–12.
[21] Yao Y, Liu Z, Xie P, Huang Z, Li T, Morris D, et al. Computationally aided, entropy-driven synthesis of highly efficient and durable multi-elemental alloy catalysts. Sci Adv 2020;6:eaaz0510.
[22] Zhang N, Feng X, Rao D, Deng X, Cai L, Qiu B, et al. Lattice oxygen activation enabled by high-valence metal sites for enhanced water oxidation. Nat Commun 2020;11:1–11.
[23] Pedersen JK, Batchelor TA, Bagger A, Rossmeisl J. High-entropy alloys as catalysts for the CO_2 and CO reduction reactions. ACS Catal 2020;10:2169–76.
[24] Ferrari A, Körmann F. Surface segregation in Cr-Mn-Fe-Co-Ni high entropy alloys. Appl Surf Sci 2020;533:147471.
[25] Ruban AV. On segregation in multicomponent alloys: surface segregation in austenite and FeCrCoNiMn alloys. Comput Mater Sci 2021;187:110080.
[26] 2020. T. Batchelor, private correspondence.
[27] Batchelor TA, Löffler T, Xiao B, Krysiak OA, Strotkötter V, Pedersen JK, et al. Complex solid solution electrocatalyst discovery by computational prediction and high-throughput experimentation. Angew Chem Int Ed 2020. https://doi.org/10.1002/anie.202014374.
[28] Ruban A, Skriver HL, Nørskov JK. Surface segregation energies in transition-metal alloys. Phys Rev B 1999;59:15990.
[29] Rogal J, Reuter K. Ab initio atomistic thermodynamics for surfaces: a primer, Technical Report, Max-Planck-Gesellschaft zur Förderung der Wissenschaften e.V. 2006. Berlin (Germany).
[30] Blöchl PE. Projector augmented-wave method. Phys Rev B 1994;50:17953.
[31] Kresse G, Joubert D. From ultrasoft pseudopotentials to the projector augmented-wave method. Phys Rev B 1999;59:1758.
[32] Kresse G, Hafner J. Ab initio molecular dynamics for liquid metals. Phys Rev B 1993;47:558.
[33] Kresse G, Furthmüller J. Efficiency of ab-initio total energy calculations for metals and semiconductors using a plane-wave basis set. Comput Mater Sci 1996;6:15–50.
[34] Kresse G, Furthmüller J. Efficient iterative schemes for ab initio total-energy calculations using a plane-wave basis set. Phys Rev B 1996;54:11169.
[35] Perdew JP, Burke K, Ernzerhof M. Generalized gradient approximation made simple. Phys Rev Lett 1996;77:3865.
[36] Murnaghan F. The compressibility of media under extreme pressures. PNAS 1944;30:244.
[37] Birch F. Finite elastic strain of cubic crystals. Phys Rev 1947;71:809.
[38] Li W-X, Stampfl C, Scheffler M. Oxygen adsorption on Ag (111): a density-functional theory investigation. Phys Rev B 2002;65:075407.
[39] Sutton AP. Electronic structure of materials. Clarendon Press; 1993.